Study on Method of Electricity and Heat Storage Planning Based on Energy Demand and Tidal Flow Velocity Forecasts for a Tidal Microgrid

Shin'ya Obara
Kitami Institute of Technology, Power Engineering Lab., Dep. of Electrical and Electronic Engineering
Koen-cho 165, Kitami, Hokkaido 090-8507, Japan
obara@mail.kitami-it.ac.jp
PHONE/FAX: +81-157-26-9262

Yuta Morizane
Kitami Institute of Technology, Power Engineering Lab., Dep. of Electrical and Electronic Engineering

Jorge Morel
Kitami Institute of Technology, Power Engineering Lab., Dep. of Electrical and Electronic Engineering

Abstract

The rapid tidal current near a lake inlet is transformed into electrical energy with Darius-type hydraulic turbine generators. When the tidal power generation is insufficient, the stored excess electric power generated from midnight to early morning of a representative day is used. The balance of energy supply and demand for all sampling events in a representative day must be predicted very accurately in a system with energy storage. In this study, electric power and heat demand are forecasted on the basis of weather data obtained from the Internet, and the corresponding values are used to plan the storage of electricity and heat from midnight to early morning. The results of the case analysis show the influence of the economic efficiency of the heating system, the capacity of the tidal power generator, the prediction error of the tidal power generator, and the insulation efficiency (Q-value) on the energy cost. Optimization of the introduced simulation model was considered. The objective functions of optimization were minimization of operation cost and facilities cost of the simulation model.

Keywords: Local energy, Tidal power generation, Microgrid, Energy storage, Numerical simulation, Operation analysis

1. Introduction

It is expected that the spread of distributed power supply systems will contribute to the expansion of green energy and the development of new town planning. However, because maintenance costs of using several facilities will be required if electric power is supplied from conventional, large-scale electric-power systems (e.g., nuclear power generation) to distant areas with low population densities, the unit price of electric power will increase. Moreover, it is economically difficult to introduce an electric power grid with the same high reliability in areas with low population density than in urban areas. However, when a distributed energy system of local supply and local consumption is introduced into an area of low population density or low energy demand, the potential arises for reducing the size of the transmission network, the unit price of electric power in the urban area, and environmental impacts. Because many researchers believed that producing energy using fossil fuels or nuclear power was lesser expensive than using green alternatives, the development of local, green energy systems in Japan has been drastically slow until recently. However, considering the sharp rise in nuclear power generation issues, the increasing cost of fossil fuels, and the energy security necessity, distributed power supplies using local energy can be introduced on a larger scale.

Therefore, this study proposes a system that connects a tidal power generator and an existing commercial electric power, and further develops the economics of the system. If a microgrid is constituted from a tidal power generator and electrical storage equipment, a stable supply of energy is technically feasible. However, because electrical storage equipment is expensive, connecting a commercial power system with a tidal power generator is more effective. To contribute to the load leveling of the commercial electric-power system when connecting a tidal power generator with a commercial electric power, the short-term power of the tidal power generator is used and electrical storage is purchased from midnight to early morning. Generally, when load leveling during the day and night, the electric power company receives an off-peak discount for service during the off-peak time (i.e., from midnight to early morning). In this study, TZPC is defined by the valid time zone for the off-peak time discount is the time zone of power rate cuts (i.e., from midnight to early morning), and CDME is defined by the discount service is the power cost discount from midnight to early morning. Many previous studies have demonstrated the use of tidal power generation [1-14].

However, examples of a tidal power generation microgrid using the CDME of commercial electric power are not available. In the controller of the proposed system, the amount of tidal power generated, the amount of electric power required, and the heat demand of a representative day are predicted, and electricity storage is planned from the relationship between the prediction results and energy balance using the CDME. When planning for the required electrical storage is inaccurate (i.e., there is insufficient amount of energy), expensive commercial electric power other than CDME will be purchased and the economic efficiency of the proposed system will decrease. To improve the accuracy of the electrical storage plan, weather forecast information is input into the controller of the proposed system using Internet data.

In an example analysis, electric power and heat are supplied to two towns and harbor facilities, supposing the introduction of a tidal power generator to Saroma Lake in Japan (Saroma Lake microgrid). The heat pump system and electric storage heaters are introduced as heat equipment because the area surrounding Saroma Lake is cold; the maximum heat demand in one day during winter is 11 times the electricity demand. Therefore, the plan to purchase commercial electric power in the TZPC must predict heat demand (space heating) with high accuracy. The Q-value (heat loss coefficient) [15] is the insulation performance of the building. The error of the outside air temperature using weather forecast information considers the temperature change from the heat demand of the building. The case analysis of the Saroma Lake microgrid clarifies comparisons of the heating system and economic efficiency, the capacity of a tidal power generator and economic efficiency, and the influence of the prediction error of the system controller on energy cost.

2. System configuration

2.1. Saroma Lake microgrid

Saroma Lake in Hokkaido is the third largest lake in Japan; the lake has a rich natural environment and is an important archeological area, including the Sea of Okhotsk and Ainu cultures. Because there is no large-scale electric power plant in the surrounding area, electric power is supplied by a nuclear power station and thermoelectric power plant hundreds of kilometers away. Therefore, it is thought that reducing the amount of power transmitted to the area by introducing a distributed power supply would significantly reduce the facilities and maintenance costs of the electrical power system. In this study, the operation of a system connecting a tidal power generator and a commercial electric power is investigated using the high-speed tidal current in the two inlets of Saroma Lake.

The outline of Saroma Lake is shown in Fig. 1. The first lake inlet is approximately 300 m wide, and the second is approximately 75 m wide. A stable tidal current exists in these inlets, and the flow velocity of this tidal current is drastically faster than that of the open sea. Figure 2 shows an example of a finite element analysis showing the tidal-current vectors near both lake inlets. The tidal-current vector is reversed by the flood and ebb tides, resulting in two to five peaks in the speed of the tidal current in one day. As shown in Fig. 1, a tidal power generation system is installed throughout the sea in these lake inlets, and a microgrid that supplies electric power and heat to the surrounding towns (Toetoko and Sakaeura) and harbor facilities is planned. The overall length of the power transmission line of the Saroma Lake microgrid is 25 km. Because the speed of the tidal current is cyclic, a compound energy system using tidal power generation, commercial electric power, and energy storage (electricity and heat storage) is developed. The Saroma Lake microgrid, used to control the compound power system, is described below.

2.2. Model of the system

Figure 3 shows the model of the Saroma Lake microgrid prepared by MATLAB/Simulink R 2012a (The Mathworks, Inc., Natick, MA, USA). The left side of the figure shows the power sources and storage battery from bus line SC_tp, and the right side shows the power load and heat storage system. Two or more tidal power generators and commercial electric power, consisting of a blade and three-phase tidal power generator, are used as the supply (power source). A snubber circuit, power conditioner [consisting of alternating current (AC)/direct current (DC), DC/DC, and an inverter], and harmonic filter are installed in each tidal power generator; the stability and quality of the AC power of bus line SC_tp are controlled. The battery can store electricity and discharge electric power to the transmission network at any arbitrary time. In addition to electricity demand, the power load experiences electric power consumption by the heat equipment. A heat pump system or electric storage heaters are introduced as heat equipment. Electric power is supplied to an electric motor to operate a compressor for the heat pump, and it is also supplied to a heat storage medium (electric resistance body) in the electric storage heater.

2.3. Energy flow of the system and plan for the operation method

2.3.1. Energy flow

The characteristics of each operational method and corresponding economic efficiency are independently analyzed. The two operational methods represent different heat supply methods: (i)

use of a heat pump system and (ii) use of an electric storage heater system. Figure 4 shows the flow of electric power and heat in the Saroma Lake microgrid system and the input/output signal of the system controller. Figure 4 (a) shows a flow chart of the heat pump system and Fig. 4 (b) shows a flow chart of the electric storage heater system. The surplus power of the microgrid's tidal power generator with the heat pump system can be supplied to the heat pump system and battery. In addition, commercial electric power can be supplied to the demand side, heat pump, and battery. Heat from the heat pump is supplied to a heat storage tank when storage is needed. When supplying heat to the demand side, the heat medium of the heat storage tank is supplied to the heat pump. Figure 4 (b) provides a flow chart of the electric storage heater system. The circulating pumps for the heat storage tank and heat medium are not used by the electric storage heater system. The electric storage heater system, used for all homes that are supplied with electricity, is safe and requires little maintenance. The energy flow described above is controlled by the computer system shown in Figs. 4 (a) and 4 (b) with an optimization program based on weather forecast information. Details of the optimization program are provided in the next section.

2.3.2. Operational control using the control computer

On the basis of the balance equations of the weather forecast data and the external electric power and heat inputs, the amount of electrical and heat storage required in the TZPC are predicted using the control computer. The amount of electrical storage and heat storage required in the TZPC (as measured from midnight the previous day (Day_{p-1}) of a representative day (Day_p) to the early morning of Day_p) are predicted on the basis of the results of an operational analysis of the system from the TZPC of one representative day to the TZPC of the next day, as shown in Fig. 5. To determine the optimal amount of electrical and heat storage, it is necessary to forecast the electric power demand, heat demand, and electricity produced by the tidal power generator as accurately as possible. In time periods other than the TZPC, the control computer uses real-time control based on a balance of actual energy supply and demand. The operational plan in the TZPC and details of the real-time control are described below.

2.3.3. Operational planning

Weather forecast information is incorporated in the planning of the TZPC from the Internet, using commands from the control computer. The weather forecast information for representative day Day_p includes outside air temperature and tide data (i.e., the difference of the sea-level height

of Saroma Lake and the open sea) for every sampling period until the next TZPC. Outside air temperature affects the predictive accuracy of the energy demand of the buildings connected to the microgrid; tide data are required to predict the electricity produced by the tidal current. From the predicted results of energy demand and electricity produced by a tidal power generator and the energy-balance equations, the amount of electric power and heat storage for every sampling period from the TZPC of the representative day Day_p to the next TZPC is estimated. When the storage of electricity and heat for every sampling period is estimated, the amount of electric power and heat stored in the TZPC is estimated by the control computer. The quantity of commercial electric power purchased is at a minimum and the economic efficiency of running the proposed system is at a maximum when the predicted energy demand and the electricity produced by the tidal power generator are equal (i.e., the stored energy exactly meets the need). However, when a prediction error is included in the system operating plan, the following economic demerits exist.

(1) Electricity storage

Figure 6 shows the predictive model of the operation method of proposal system in this study. The surplus power of the energy balance in Fig. 6 is taken into consideration by the amount of charge to the battery in the TZPC. Accordingly, when electric power of tidal power generation exceeds the amount demanded by forecast of the supply-and-demand balance, the surplus power is used by storage of electricity with a time shift. Therefore, surplus power is not sold to a commercial system. A surplus of electricity results in an increase in the amount of self-discharge, an increase in electrical storage loss, and an increase in the required battery capacity of the facility. A shortage of stored electricity leads to the need to purchase commercial electric power at more expensive electric-power unit prices than the CDME.

(2) Heat storage

An operating surplus of heat storage results in an increase in both the heat radiation and the required capacity of the heat storage tank. A shortage of heating energy during operation results in the need to purchase commercial electric power at more expensive electric-power unit prices than the CDME in order to supply to heat pumps or electric storage heaters.

Figure 6 presents a schematic of electricity storage in the Saroma Lake microgrid. TZPC (1) represents the time zone from midnight on day Day_{p-1} preceding the representative day Day_p to the early morning of Day_p. The control computer instructs the storage of electricity during each

TZPC. From the electric power provided by the tidal power generators (area shaded in blue) and previously stored electricity and subsequent discharge (white- and red-hatched areas), the electricity demand (dashed line) of time zones other than the TZPC is provided. When the predicted energy demand and electricity produced by the tidal power generator are equal, the white- and red-hatched areas will reach zero just before the start time of the next TZPC (blue circles). However, if there is more electricity stored than needed, the white- and red-hatched areas will maintain a positive value at the start time of the next TZPC. Additionally, when there is insufficient stored electricity, the white- and red-hatched areas will reach zero prior to the start time of the next TZPC.

2.4. Error following the operational plan

2.4.1. Prediction error of the weather forecast information and heat demand

Figure 7 shows the correct hit rate of rainfall prediction from the Meteorological Agency of Japan from 2004 to 2012 (Fig. 7 (a)) and the error of the forecasted outside air temperature (Fig. 7 (b)) for the same period [16]. The hit rate of rainfall probability over the nine-year period ranges from 68% to 89% and that averaged over a year is approximately 80%. The forecast error of outside air temperature gradually decreases, and the errors in the minimum and maximum temperatures in 2011 and 2012 are 1.8 °C and 2.0 °C, respectively.

The Q-value [W/(m²·K)], also called the heat loss coefficient [15], is a measure of the insulation efficiency of a building, defined by dividing the heat loss of the building by the architectural area. Although the average Q-value of residences in the Saroma Lake neighborhood is approximately 2.33 W/(m²·K), newer residences often achieve insulation efficiencies near 1.0. If the Q-value is represented by the average floor area of a building is $\overline{S}$, the prediction error of the outside air temperature is $\Delta\dot{t}$, and the heat load of the space heating of the building is $\dot{h}_{sh}$, then the error $\Delta\dot{q}_{sh}$ of the heat demand using space heating is calculated using Eq. (1) as follows:

$$\Delta\dot{q}_{sh} = QFT \cdot \overline{S} \cdot \Delta\dot{t} / \dot{h}_{sh} \quad (1)$$

When the forecast error of the outside air temperature shown in Fig. 7 (b) is applied in Eq. (1), the error of the heat-demand forecast of space heating shown in Fig. 8 is obtained. Figure 8 shows the results of analysis for winter (February), spring (April), and summer (August). There is little heat radiation because smaller Q-values have higher insulation efficiency, leading to a fairly accurate

space heating demand based on the forecast error of outside air temperature. The error in space heating demand from the error of the weather forecast in April becomes uniform at approximately 10% in the case of Q-value = 1.6 W/(m²·K). Because the space heating demand in August is very small, for the case of Q-value = 1.6 W/(m²·K), the error in the space heating demand from the weather forecast error is approximately 0%. From Fig. 8, the error in space heating demand from the weather forecast error is a maximum of approximately 25% for every season.

The components of the power load are described by Eq. (2). The electric power load $\dot{e}_{load}$ consists of loads $\dot{e}_{nd}$, representing power loads other than heat equipment such as household appliances, and load $\dot{e}_{heat}$, which represent loads from the heat equipment. Furthermore, $\dot{e}_{heat}$ comprises load $\dot{e}_{sh}$ (the load from space heating) and load $\dot{e}_{hw}$ (the power load from the hot water supply). As described above, $\dot{e}_{sh}$ can have a maximum error of 25%. Because the prediction errors of $\dot{e}_{nd}$ and $\dot{e}_{hw}$ are small compared to those of $\dot{e}_{sh}$ in a cold region, the details are not investigated in this study.

$$\dot{e}_{load} = \dot{e}_{nd} + \dot{e}_{heat} = \dot{e}_{nd} + \left(\dot{e}_{sh} + \dot{e}_{hw}\right). \quad (2)$$

2.4.2. Prediction of the tidal power generation

Figure 9 (a) shows the test results of tide levels of the open sea (Sea of Okhotsk) and of Saroma Lake, and the difference in tide level between the sea and the lake. The tidal-current speed in August 5–19, 2010 [17] is also shown. Figure 9 (b) shows the results in August 7–10, 2010. The speed of the tidal current in Fig. 9 is the north–south component in a water depth of 6 m in the first inlet of Saroma Lake. Flow from Saroma Lake to the Sea of Okhotsk occurs during the ebb tide (flowing north) and that the Sea of Okhotsk to the Saroma Lake (flowing south) occurs during the flood tide. Tidal currents occur because a difference in tide level arises between the open sea and the lake owing to changes in the tide level of the Sea of Okhotsk. The flow velocity following the ebb and flood tides peaks two to five times each day. Because the direction of the tidal current is reversed by the flood and ebb tides, the rotation direction or direction of the tidal power generator must be reversible. The tide-level difference $\dot{L}_d$ and tidal-current speed $\dot{v}_w$ are expected to have a strong relationship; therefore, the approximate expression shown in Eq. (3) is introduced as follows:

$$\dot{v}_w = C_{lm} \cdot \left(-\dot{L}_d\right) \quad \text{where} \quad C_{lm} \quad \text{is a constant.} \tag{3}$$

253

254 C_{lm} in Eq. (3) is a proportionality factor obtained from correlation of test results for tide-level
255 difference $\dot{L}_d$ and tidal-current speed $\dot{v}_w$. When the cycle of the tide-level difference (Fig. 9 (a)) is
256 reversed and a proportionality coefficient ($C_{l,m}$ = 5.8) is given on the basis of Eq. (3), as shown in
257 Figure 10, the tidal-current speed is strongly correlated against the tide-level difference. Because
258 details of the tide-level difference at arbitrary times are released by the Coast Guard of Japan [18],
259 the speed and tidal current at any time can be easily predicted. Figure 11 shows the tidal-current
260 speed prediction for each tide-level difference $\dot{L}_d$ for February 5–19 (winter), April 5–19 (spring),
261 and August 5–19 (summer) in 2010, obtained using $C_{l,m}$ = 5.8 in Eq. (3).
262 Figure 12 shows the difference between the predicted tidal power generation integrated over each
263 day and the production of electricity obtained from the actual tidal-current speed integrated over
264 each day in August 5–19, 2010. The error range is approximately 10–25%, but a maximum value of
265 32% was recorded on August 17, 2010. Although it is easier to predict energy production for tidal
266 power generation than for photovoltaics or wind power generation, the inaccuracy of the Saroma
267 Lake microgrid in this study exceeds 30% at times.

268

269 **3. Energy-balance equations and calculation formula for economic efficiency**

270 *3.1. Power balance*

271 Equations (4) and (5) represent the power balances at a specific sampling time for the power- and
272 heat-distribution networks in the Saroma Lake microgrid. The left-hand side of Eqs. (4) and (5)
273 represents electric power outputs, and the right-hand side represents electric power consumption.
274 Commercial electric power ($\dot{e}_{cp}$), current power generators of N_{td} sets, and battery power ($\dot{e}_{bto}$)
275 are supplied to a power network by the Saroma Lake microgrid. Electric power is consumed by the
276 electricity demand ($\dot{e}_{nd}$), the accumulation of electricity in the battery ($\dot{e}_{bti}$), the heat pumps of N_{hp}
277 sets or the electric storage heaters of N_{eh} sets, and the heat loss of N_{loss} sets. As shown in Eq. (6),
278 electricity demand $\dot{e}_{nd}$ is the sum of the time-averaged electricity demands $\dot{e}_{nd,T}$ for the Toetoko
279 town of N_T residences, $\dot{e}_{nd,S}$ for the Sakaeura town of N_S residences, and electricity demand of
280 the corresponding port facilities $\dot{e}_{portT}$ and $\dot{e}_{portS}$. Heat losses at inverters and converters, and
281 power transmission losses are included in the electric-power loss $\dot{e}_{loss}$.

282

$$\dot{e}_{cp} + \sum_{i=1}^{N_{td}} \dot{e}_{td,i} + \dot{e}_{bto} = \dot{e}_{nd} + \dot{e}_{bti} + \sum_{j=1}^{N_{hp}} \dot{e}_{hp,j} + \sum_{k=1}^{N_{loss}} \dot{e}_{loss,k}, \quad (4)$$

$$\dot{e}_{cp} + \sum_{i=1}^{N_{td}} \dot{e}_{td,i} + \dot{e}_{bto} = \dot{e}_{nd} + \dot{e}_{bti} + \sum_{l=1}^{N_{eh}} \dot{e}_{eh,l} + \sum_{k=1}^{N_{loss}} \dot{e}_{loss,k}, \quad (5)$$

$$\dot{e}_{nd} = N_T \cdot \dot{e}_{nd,T} + N_S \cdot \dot{e}_{nd,S} + \dot{e}_{port,T} + \dot{e}_{port,S}. \quad (6)$$

283

284 *3.2. Heat energy equations*

285 Equations (7) and (8) are the heat balance equations for the Saroma Lake microgrid accompanied
286 by a heat-pump system and electric storage heater system, respectively. The left-hand side of Eq. (7)
287 represents the heating power of the heat pump ($\dot{h}_{hp}$) and heat storage tank ($\dot{h}_{sto}$); the right-hand
288 side includes heat demand ($\dot{h}_{nd}$), heat storage ($\dot{h}_{sti}$), and radiation loss ($\dot{h}_{loss}$). Here, $\dot{h}_{hp,j}$ is
289 $\dot{C}_j \cdot \dot{e}_{hp,j}$, where $\dot{C}_i$ is the coefficient of performance of the heat pump j and $\dot{e}_{hp,i}$ is the power
290 supply to j. In the heat-pump system, heat is stored in a heat storage tank using a heat medium; in
291 the electric storage heater system, heat is stored by turning on electricity to the electric storage
292 heaters installed in each room. The left-hand side of Eq. (8) represents the heating power of the
293 electric storage heaters ($\dot{h}_{eho}$); the right-hand side represents the heat demand ($\dot{h}_{nd}$), heat storage
294 ($\dot{h}_{ehi}$) of the electric storage heaters, and radiation loss ($\dot{h}_{loss}$). The efficiency of thermal storage in
295 the electric storage heater j is $\eta_{eh,j}$, the electric power supplied to j is $\dot{e}_{eh,j}$, and the heating value
296 that can be output from the electric storage heaters is $\dot{h}_{eho,j} = \eta_{eh,j} \cdot \dot{e}_{eh,j}$.

297

$$\sum_{j=1}^{N_{hp}} \dot{h}_{hp,j} + \dot{h}_{sto} = \sum_{j=1}^{N_{hp}} \left(\dot{C}_i \cdot \dot{e}_{hp,j}\right) + \dot{h}_{sto} = \dot{h}_{nd} + \dot{h}_{sti} + \dot{h}_{loss}, \quad (7)$$

$$\sum_{l=1}^{N_{eh}} \dot{h}_{eho,l} = \dot{h}_{nd} + \sum_{l=1}^{N_{eh}} \dot{h}_{ehi,l} + \dot{h}_{loss}. \quad (8)$$

298

299 *3.3. Calculation formula for economic efficiency*

300 With respect to the economic efficiency of the Saroma Lake microgrid, only the facilities costs and
301 power rates are considered in this study. Maintenance costs are not included in the facilities cost.
302 The equipment cost of the Saroma Lake microgrid using the heat pump system and electric storage
303 heater system is calculated using Eqs. (9) and (10), respectively. The unit prices for each piece of
304 equipment are V_{td} (a tidal power generator), V_{bt} (a battery), V_{hp} (a heat pump), V_{eh} (an electric
305 storage heater), V_{st} (a heat storage tank), L_{tl} (a transmission line), and V_{eq} (auxiliary

306 machinery, i.e., various types of converters, inverters, safety devices, and system interconnection
307 equipment and/or a control device). The total equipment cost of the heat pump system or electric
308 storage heater system is calculated using the number and unit price of each piece of equipment
309 introduced into the system.
310

$$P_{hp} = u_{td} \cdot V_{td} + u_{bt} \cdot V_{bt} + \sum_{j=1}^{N_{hp}} \left(u_{hp} \cdot V_{hp,j} \right) + u_{st} \cdot V_{st} + u_{tl} \cdot L_{tl} + \sum_{m=1}^{N_{eq}} \left(u_{eq} \cdot V_{eq} \right), \quad (9)$$

$$P_{eh} = u_{td} \cdot V_{td} + u_{bt} \cdot V_{bt} + \sum_{l=1}^{N_{eh}} \left(u_{eh} \cdot V_{eh,l} \right) + u_{tl} \cdot L_{tl} + \sum_{m=1}^{N_{eq}} \left(u_{eq} \cdot V_{eq} \right). \quad (10)$$

311
312 The purchase price of commercial electric power consists of usage charges determined by peak
313 load and a commodity charge determined by consumption. Equation (11) represents the electricity
314 rate of the Saroma Lake microgrid. The first term on the right-hand side of Eq. (11) is the electric
315 commodity charge and the second term is the monthly usage charge. The usage charge is
316 determined by the maximum load of the commercial electric power used in one year.
317

$$P_{op} = \sum_{n=1}^{N_{month}} \left(u_{uc} \cdot \dot{q}_{uc,n} \right) + \sum_{m=1}^{N_{month}} \left(P_m \right). \quad (11)$$

318
319 Figure 13 shows the commodity charge of electric power by CDME (peak-control-type electric
320 power: Dream 8) [19] of Hokkaido Electric Power Co., Inc. The unit prices [u_{uc} in Eq. (11)] of the
321 commodity charge of Dream 8 differ by season, time zone, and the quantity purchased $\dot{q}_{uc}$. The
322 time zone for low power rates, TZPC, ranges from 22:00 to 06:00 h of the next morning in this case.
323 Figure 14 shows the monthly electric-power usage charges in Dream 8. Usage charges are constant
324 when the amount of electric power used per month is 10 kWh or less. However, if the amount of
325 electric power used in a month exceeds 10 kWh, usage charges will increase in proportion to the
326 amount used.
327
328 **4. Operational example**
329 This section provides an example of providing energy to the Saroma Lake surrounding area using
330 the proposed system. As shown in Fig. 1, there are 227 households comprising 853 individuals in
331 Toetoko and Sakaeura, and there are harbor facilities around Saroma Lake in each town. In this

analysis, electric power and heat are supplied to meet the demand of the population described above using the Saroma Lake microgrid.

4.1. Energy demand

Figure 15 shows the electric power and heat demand that are supplied to a surrounding area from the Saroma Lake microgrid. The energy-demand characteristics shown in Fig. 15 were calculated from the average energy demand of Hokkaido, Japan. Moreover, the power demand of two harbor facilities was 60 kW in one year. Because the heat load of the equipment is not included in the electricity demand of the months shown in Fig. 15 (a), there is no a significant difference between the months. In the heat load shown in Fig. 15 (b), however, the magnitude of the load changes significantly each month. The heat-to-power ratios on each representative day in February, April, and August are 11.0, 5.2, and 1.0, respectively.

4.2. Analytic conditions

The characteristics of the equipment used in the Saroma Lake microgrid are listed in Table 1. Table 2 provides the unit prices of the equipment used in the analysis based on current pricing. In the operational analysis of the system, both the heat-pump system and electric-storage heater system are analyzed. The tidal power generators, a battery, heat pumps or electric storage heaters, and a heat-storage tank are included in the equipment cost, but the transmission line and auxiliary machinery are not included.

4.3. Method of operation

The time zone of the TZPC by application of the CDME is set from 22:00 to 06:00 h of the next day, assuming the same rate structure as Dream 8 of Hokkaido Electric Power Co., Inc. shown in Figures 13 and 14. The pattern of electricity and heat demand is shown in Fig. 15. Although heating demand takes a large power load, the prediction error of the heating demand is set to 40% of the maximum in order to exceed the results of the investigation shown in Fig. 8. The prediction error of the tidal power generator is set to 40% of the maximum, exceeding the 33% maximum error shown in Fig. 12. The prediction error of the power demand and tidal power generation is modeled by adding the error by a random number to the characteristics shown in Figs. 11 and 15.

Figure 16 shows the analysis flow of the proposed system. The analysis consists of three steps (STEP 1–3). The power demand (ΔE_{day_p}), heat demand (ΔH_{day_p}), and tidal power generation

(E_{td,day_p}) from 22:00 h on the previous day (Day_{p-1}) of representative day (Day_p) to 22:00 h on Day_p (24 h from the TZPC start time of Day_{p-1} to just before the TZPC start time of Day_p) are predicted using Eqs. (12) and (13) in STEP 1. However, the kinetic energy of the tidal power generator ($\dot{p}_w$) is defined as the inflow mass (m_w) of the tidal current to area *S* for 1 s; the speed of the tidal current is $\dot{v}_w$, calculated by Eq. (14). The data from the 5th to 19th of every month, shown in Fig. 11, are used for the tidal-current speed in Eq. (14). The quantity of electric power to be stored, E_{bt,day_p}, predicted by STEP 1, is charged to $\dot{e}_{bti}$ in STEP 2 in the time range of the TZPC (8 h), as shown in Eq. (15). As shown in Eq. (16), the power supply ($\dot{e}_{sti}$) for heat storage during the TZPC changes with the use of a heat-pump system or electric storage heater system.

$$E_{bt,day\_p} = \Delta E_{day\_p} - E_{td,day\_p} + \Delta E_{loss,day\_p}, \tag{12}$$

$$H_{st,day\_p} = \Delta H_{day\_p} + \Delta H_{loss,day\_p}, \tag{13}$$

$$\dot{p}_w = \frac{1}{2} \cdot m_w \cdot \dot{v}_w^{\,2} \quad \text{where,} \quad m_w = \rho_w \cdot S \cdot v_w, \tag{14}$$

$$\dot{e}_{bti} = \left(E_{bt,day\_p} / \eta_{cd}\right)/8. \tag{15}$$

In the case of the heat pump system, $\dot{e}_{sti} = \left(H_{st,day\_p} / \dot{C}\right)/8$. (16)

In the case of the electric storage heater system, $\dot{e}_{sti} = H_{st,day\_p}/8$.

Control in actual time is assumed in STEP 3. In real-time control, when the energy-balance equations [from Eq. (4) to Eq. (8)] of electric power and heat are not filled with a sufficient amount of accumulated electricity or heat, the control computer orders the purchase of commercial electric power. The purchase of commercial electric power during a time range other than the TZPC leads to an increase in energy cost. The objective function of the system is minimization of the power rates shown in Eq. (11). Accordingly, the economic efficiency of a system is evaluated in the sum total of the electric commodity charge and the monthly usage charge.

5. Results of the operational example

5.1. Operational method and economic efficiency

Figure 17 shows the results of the operational analysis of the Saroma Lake microgrid accompanied by the heat pump system in February (winter), April (spring), and August (summer) of a typical year. Figure 18 shows the results of the system accompanied by the electric storage heaters. One hundred sets of tidal power generators are introduced in the analytic results shown in

Figs. 17 and 18 (a–d), which illustrate the quantities of electric power purchased (apparent power), electricity accumulated, and heat stored, and the ratio of tidal power generation to the electric power supply. Operations of energy storage are the method shown in Fig. 16. In the analysis described in Section 4.3, the initial values of the amount of electricity accumulated and heat stored are set to zero, and a significant amount of electric power is purchased in the TZPC on the first day of each month. Owing to a large change in tidal-current speed during April 15–17, 2010 (shown in Fig. 11) and low heat demand in spring, the accumulation of electricity significantly changes after April 15. The time zone that shows a negative accumulation of electricity in Figs. 17 (b) and 18 (b) occurs during the TZPC, and the control computer commands the system to accumulate electricity by purchasing electric power via the CDME. A large load (charge and discharge) is added to a battery according to the characteristics of both the load and tidal-current speed. Figs. 17 (c) and 18 (c) show the operational results of heat storage. Because a heat storage loss occurs in the heat-storage tank of the system using the heat pump, heat-storage capacity becomes greater in this system than in the system using the electric storage heater. Figures 17 (d) and 18 (d) show the ratio of the tidal power generation ($\sum_{i=1}^{N_{td}} \dot{e}_{td,i}$ in the representative day) to the power load (electric power used in E_{bt,day_p} and H_{st,day_p}) of the representative day. For a significant heat demand to be required in February, the ratio of tidal power generation to power load is low. The tidal-current speed during the period April 15–19 is large (Fig. 11 (b)) and the heat demand is small, causing the ratio of tidal power generation to demand to be extremely high.

5.2. Amount of tidal power generation introduced and economic efficiency

Figure 19 shows the analytical results of the commodity charge (usage charges not included) of electric power for operation of the proposed system with 100 sets of tidal power generators. The purchase charges for electric power in the system containing the electric storage heater are 2.8, 2.2, and 1.2 times that of the system containing the heat pump in February, April, and August, respectively. Introduction of the heat pump system in cold regions is highly effective in reducing the electric-power commodity charge.

Figure 20 shows the number of tidal power generators installed, the analytical results of the electricity rate in each month, and the equipment cost. The usage charges for commercial electric power are generally the same over a one-year cycle; usage charges (Fig. 14) fixed from the maximum monthly load are shown in Fig. 20. Compared to the power rates, the equipment cost is

significant. In particular, the battery requirement and the cost of the heat equipment required to satisfy the heat demand in February are both large. When supplying the same amount of energy as the proposed system with a conventional commercial electric power supply with a heat pump system of COP = 3.5 (see left-hand side of Fig. 20), the costs are as follows: 9.3 × 10^6 JPY, 5.7 × 10^6 JPY, and 3.4 × 10^6 JPY (usage charges 1,627.5 JPY/month-building) in February, April, and August, respectively. A unit price of 25.37 JPY/kWh was used for electric power in the calculations. Because the purchase of commercial electric power will decrease when the number of tidal power generators installed increases (Fig. 20), the power rates of the proposed system decrease. The system with the heat pump requires lesser commercial electric power to be purchased than the system with the electric storage heater. However, numerous tidal power generators must be introduced for the power rates of the proposed system with electric storage heaters to be lesser than those of the conventional system. At the equipment cost shown in the right-hand side of Fig. 20, the battery capacity for storing electric power by tidal power generation increases, requiring additional tidal power generators to be introduced into the system. Moreover, the equipment cost of the electric storage heater system is significantly lower than that of the heat pump system. Even if the difference in the purchase cost of commercial electric power is considered, the difference in the equipment cost described above is irrecoverable for decades. In other words, the equipment cost of the proposed system is significantly higher than the purchase price of commercial electric power. Therefore, with the present equipment costs, the superiority or inferiority of the proposed system is decided by the magnitude of the equipment cost rather than by the difference in the quantity of commercial electric power purchased. Although there are fewer occasions to purchase commercial electric power using the heat pump system compared to the electric storage heater system, when equipment cost is considered, the electric storage heater is advantageous from an economic perspective. Realization of the proposed system is strongly controlled by equipment costs, the magnitude of which depends strongly on the costs of the battery and tidal power generators in addition to the cost of the heat equipment.

5.3. Prediction error of energy demand and influence on economic efficiency

Figure 21 shows the results of examination of the influence of the commodity charge on electric power by the prediction error of electricity demand and heat demand. Because power consumption by the electric storage heater is larger than that of a heat pump under the same space-heating load, the influence of prediction error is greater in the system with electric storage heaters. In the electric

storage heater system, the prediction error range is 40% of the electricity and heat demand, and the maximum purchase error of commercial electric power is 12%. In contrast, the maximum purchase error of commercial electric power is 3.5% for the heat pump system.

Figure 22 shows the results of the examination of the influence of the tidal power generation prediction error on the commodity charge of electric power. As shown in Fig. 21, the system accompanied by the electric storage heaters is more affected by the influence of the tidal power generation prediction error than is the proposed heat pump system. For the electric storage heater system, when the prediction error of the electricity produced by tidal power generation is 40%, the maximum purchase error of commercial electric power is 11.5%. In contrast, the maximum purchase error of the commercial electric power for the heat pump system is 3.9%. These results indicate that prediction error affected the proposed system with the heat pump significantly lesser than the system with the electric storage heater.

6. Conclusions

Introduction of the proposed microgrid into a cold region with a large heat-to-power ratio was investigated by numerical analysis, from which the following conclusions were obtained.

(1) Because buildings differ in insulation efficiency, space-heating loads also differ for a given outdoor air temperature. Thus, in this study, the magnitudes of the building heat loads were calculated by introducing the heat loss coefficient (Q-value). From the results described previously and the magnitude of the error of current weather forecast information (outside air temperature), the prediction error of the space heating load of buildings was estimated (with a maximum value of 27.5%). Next, the load change (40%) exceeding the maximum error was applied to the proposed system at random, showing the influence of the quantity of commercial electric power purchased. In the range of a 40% prediction error in space-heating load, the maximum purchase error of commercial electric power was 12% for the system containing an electric storage heater and 3.5% for the system using heat pumps. The proposed system with heat pumps is fairly insensitive to the prediction error of weather-forecast information.

(2) When the number of tidal power generators increases, the battery capacity for storing the electric power of the generators also increases. Although the purchase of commercial electric power in the system with heat pumps is lower than that in the system with an electric storage heater, the equipment cost begins to negate that advantage. The difference in the equipment cost described here is significant compared to the difference in the purchase cost of commercial electric power.

Therefore, with the current cost of the heat equipment used in the proposed system, introduction of electric storage heaters is advantageous. Because the equipment cost of the system proposed in this study is much higher than the purchase price of commercial electric power, realization of the proposed system is strongly controlled by the equipment cost. Careful development of the heat equipment, battery, and tidal power generator, and minimization of equipment cost are crucial to realization of the system.

(3) Because the power supply in the system with electric storage heaters is larger than that of the heat pump system under the same space heating load, the prediction error of the amount of electricity produced by the tidal power generator has a greater effect on the system with the electric storage heater than on the system with heat pumps. When the prediction error of the tidal power generation of the system with the electric storage heaters was in the range of 40%, the purchase error of commercial electric power was the maximum, 11.5%. In contrast, the maximum prediction error in the system with heat pumps was 3.9%. The proposed system with heat pumps is insensitive to the prediction error of energy demand and supply compared to the system with electric storage heaters.

Nomenclature

$\dot{C}$	:	Coefficient of performance of the heat pump
C_{lm}	:	Constant
Day_p	:	Representative day
E_{bt,day_p}	:	Energy to be stored in the battery on a representative day [kWh]
E_{td,day_p}	:	Tidal power generation of a representative day [kWh]
ΔE_{day_p}	:	Electricity demand of a representative day [kWh]
$\Delta E_{loss,day\_p}$	:	Electricity loss of a representative day [kWh]
$\dot{e}$	:	Electric power load [kW]
H_{st,day_p}	:	Heat storage of a representative day [kWh]
ΔH_{day_p}	:	Heat demand of a representative day [kWh]
$\Delta H_{loss,day\_p}$	:	The heat loss in a representative day [kWh]
$\dot{h}$	:	Heat load [kW]
$\Delta\dot{h}_{sh}$	:	Heat load of space heating [kW]
JPY	:	Japanese Yen [Yen]

$\dot{L}_d$: Tide level difference [m]

L_{tl} : Unit price of transmission line [JPY/m]

m_w : Mass [kg]

N : Number

P : Cost [JPY]

P_m : Usage charges [JPY]

$\dot{P}_w$: Kinetic energy [kW]

QFT : Q-value [kW/(m²·K)]

$\Delta\dot{q}_{sh}$: Error of the heat demand of space heating

$\dot{q}_{uc}$: Amount of electricity used [JPY/kWh]

S : Channel area [m²]

$\overline{S}$: Floor area of buildings in the service area [m²]

$\Delta\dot{t}$: Maximum predicted error of the outdoor air temperature [K]

u : Amount of introduction

u_{uc} : Unit price of power [JPY]

V : Unit price [JPY]

$\dot{v}_w$: Tidal-current speed [m/s]

Greek characters

ρ_w : Density of seawater [kg/m³]

η : Efficiency

Subscripts

bt : Battery

bti : Battery charge

bto : Battery discharge

cd : Charge and discharge of the battery

cp : Commercial power

eh : Electric storage heater

ehi : Charge of the electric storage heater

eho : Output of the electric storage heater

eq : Auxiliary machinery

heat : Heat

hp : Heat pump

hw : Hot water supply

load : Load

loss : Loss

nd : Demand

op	:	Electric charges (Commodity and usage charges)
port	:	Port
S	:	Sakaeura town
sh	:	Space heating
st	:	Heat storage tank
sti	:	Heat input to the heat storage tank
sto	:	Heat output from the heat storage tank
T	:	Toetoko town
td	:	Tidal

References

[1] Obara S, Kawai O, Kawae Y. Morizane Y. Operational planning of an independent microgrid containing tidal power generators, SOFCs, and photovoltaics. Appl. Energy 2013;102: 1343-1357.

[2] Georgios M. Kopanos, Michael C. Georgiadis, Efstratios N. Pistikopoulos, Energy production planning of a network of micro combined heat and power generators. Appl. Energy 2013;102:1522-1534.

[3] Marzband M, Sumper A, Ruiz-Álvarez A, Luis J, Domínguez-García, Tomoiaga B. Experimental evaluation of a real time energy management system for stand-alone microgrids in day-ahead markets. Appl. Energy, 2013;106:365-376.

[4] Manfren M, Caputo P, Costa G. Paradigm shift in urban energy systems through distributed generation: Methods and models, Appl. Energy 2011;88:1032-1048.

[5] Ren H, Gao W. A MILP model for integrated plan and evaluation of distributed energy systems, Appl. Energy 2010;87:1001-1014.

[6] Zhang P, Li W, Li S, Wang Y, Xiao W. Reliability assessment of photovoltaic power systems: Review of current status and future perspectives. Appl. Energy 2013;104:822-833.

[7] Junqiang X, Roger AF, Binliang L. Impact of different operating modes for a Severn Barrage on the tidal power and flood inundation in the Severn Estuary, UK: Appl. Energy 2010; 87: 2374–2391.

[8] Paul AW, Kevin AH, Zafer D, Thomas G. Tidal stream energy site assessment via three-dimensional model and measurements. Appl. Energy 2013; 102: 510–519.

[9] Kyozuka Y. An experimental study on the Darrieus-Savonius turbine for the tidal current power generation. JSME J. Fluid Science and Technology 2008; 3: 439–449.

[10] Deog HD, Suzuki K. Power generation characteristics of a novel horizontal tidal current power generation system installed in the Akashi Strait of Japan. Sustainable Energy Technologies (ICSET), IEEE International Conference 2010; 1–6.

[11] Dolman S, Simmonds M. Towards best environmental practice for cetacean conservation in developing Scotland's marine. Renewable Energy 2010; 34: 1021–1027.

[12] Johnson K, Kerr S, Side J, Accommodating wave and tidal energy–Control and decision in Scotland. Ocean & Coastal Management 2012; 65: 26–33.

[13] Bae YH, Kim KO, Choi BH, Lake Sihwa tidal power plant project. Ocean Engineering 2010; 37: 454–463.
[14] Lee DS, Oh SH, Yi JY, Park W, Cho HS, Kim DG, et al., Experimental investigation on the relationship between sluice caisson shape of tidal power plant and the water discharge capability. Renewable Energy 2010; 35: 2243–2256.
[15] Takeda-Kindaichi S, Nagano K, Katsura T, Hori S, Shibata K. Annual energy consumption in an actual low energy house in the cold region of Japan. Proceedings of the 4th experts meeting and workshop of IEA HPP Annex 32. Kyoto 2007; 1–22.
[16] Homepage of Japan Metrological Agency. http://www.data.jma.go.jp/obd/stats/etrn/index.php, 2012.
[17] Abashiri development and construction department, Hokkaido regional development bureau report on investigation of flow regime of Lake Saroma fishing port, and other work 2010. in Japanese.
[18] Japan Oceanographic Data Center, Hydrographic and Oceanographic Department, Japan Coast Guard, http://www1.kaiho.mlit.go.jp/jhd-E.html, 2012.
[19] Hokkaido Electric Power Co., Inc., Light according to the peak restraint type time. http://www.hepco.co.jp/userate/price/ratemenu/menu_regular/02.html, 2012.

565 **Figure and table captions**

566

Fig. 16 Operational method of the proposed microgrid system

Fig. 17 Results of analysis of the Saroma Lake microgrid with 100 sets of tidal power generators and a heat pump system

(a) Purchase of apparent power during three seasons

(b) Electric power storage

(c) Heat power

(d) Ratio of tidal power generation to electricity demand

Fig. 18 Results of analysis of the Saroma Lake microgrid with 100 sets of tidal power generators and an electric storage heater system.

(a) Purchase of apparent power during three seasons

(b) Electric power storage

(c) Heat power

(d) Ratio of tidal power generation to electricity demand

Fig. 19 Electric power purchase price (commodity charge) during three seasons. Usage charges are not included. System includes 100 sets of tidal power generators.

(a) With heat pump system

(b) With electric storage heater system

Fig. 20 Results of analysis of electricity charges and equipment costs.

(a) 20 sets of tidal power generators

(b) 100 sets of tidal power generators

(c) 200 sets of tidal power generators

Fig. 21 Example of the relationship between prediction error of power and heat demand, and change in the commodity charge of power

Fig. 22 Example of the relationship between prediction error of tidal current power and change in the commodity charge of power

Table 1 Characteristics of the equipment

Table 2 Unit prices of equipment

629 Fig. 1

630

631

632

633

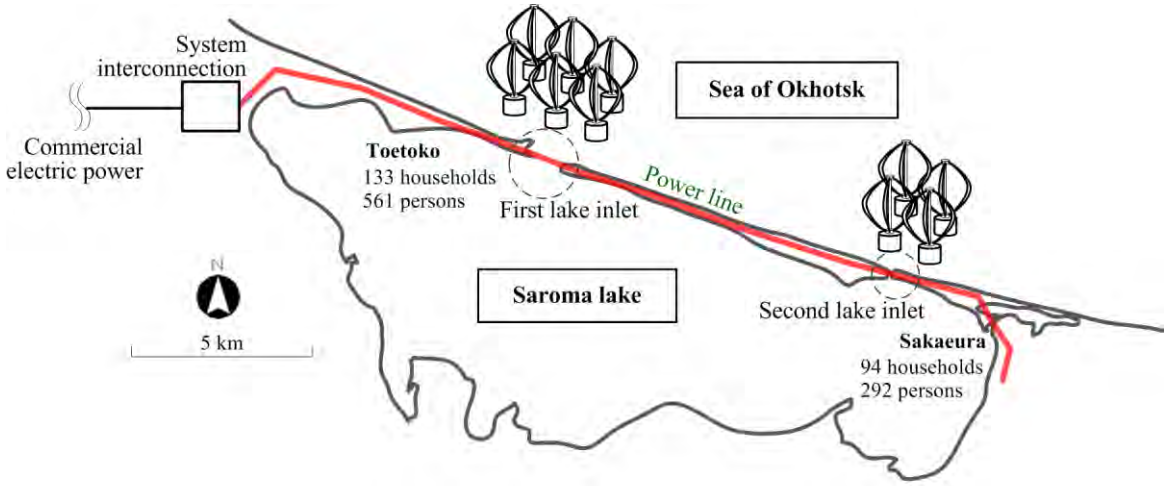

Area	151.82km²	Origin	Inland sea-lake
Boundary length	87 km	Water	Brackish water
Maximum water depth	19.6 m	Type of lake and marsh	Eutrophic lake
Mean water depth	8.7 m	Transparency	9.4 m
Storage capacity	1.3 km³		

634

635

636

637

638

639

640

641

642

643

644

645

646

647

648

649

Fig. 2

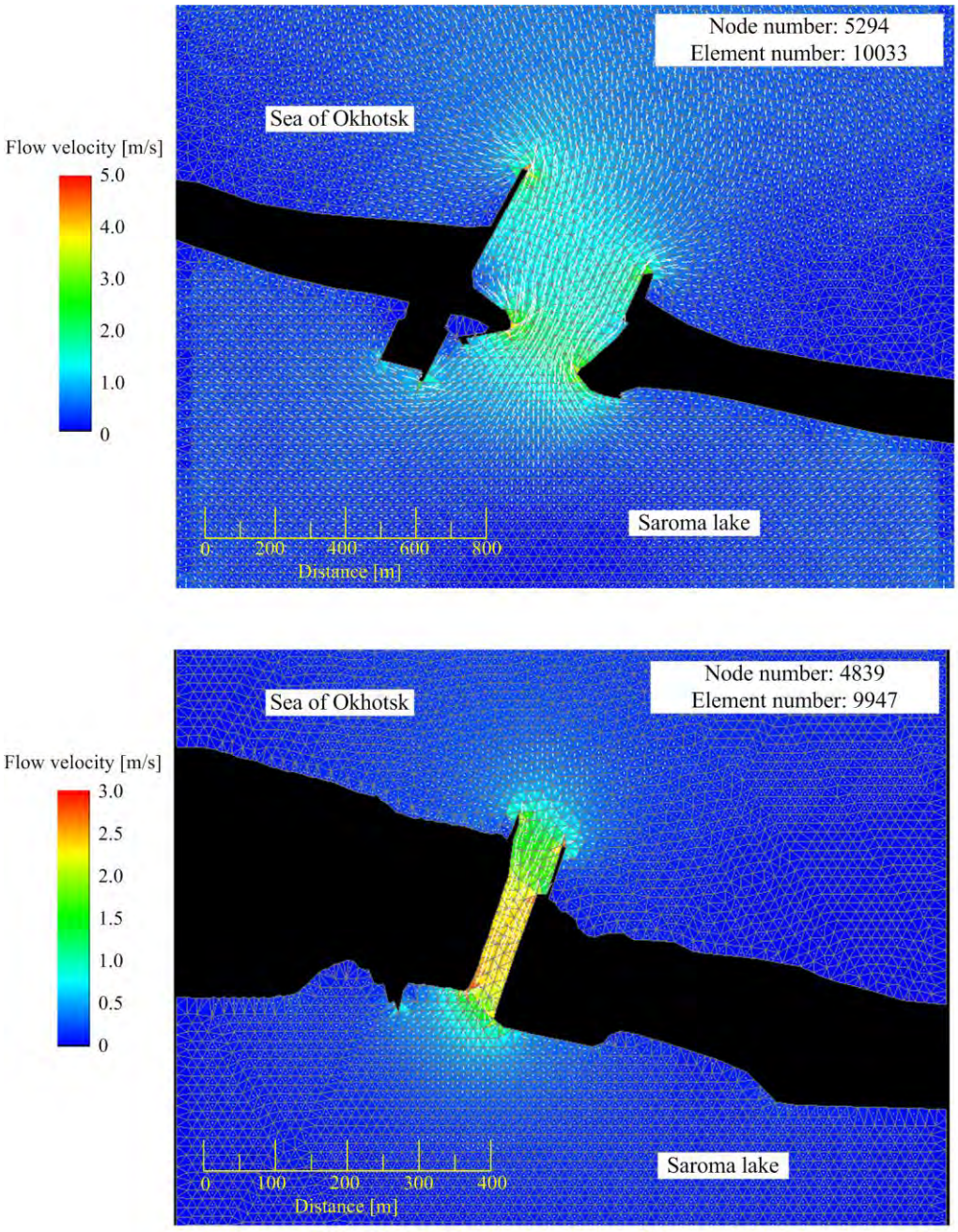
Node number: 5294
Element number: 10033
Sea of Okhotsk
Flow velocity [m/s]
5.0
4.0
3.0
2.0
1.0
0
0
200
400
600
800
Distance [m]
Saroma lake
Node number: 4839
Element number: 9947
Sea of Okhotsk
Flow velocity [m/s]
3.0
2.5
2.0
1.5
1.0
0.5
0
0
100
200
300
400
Distance [m]
Saroma lake

Fig. 3

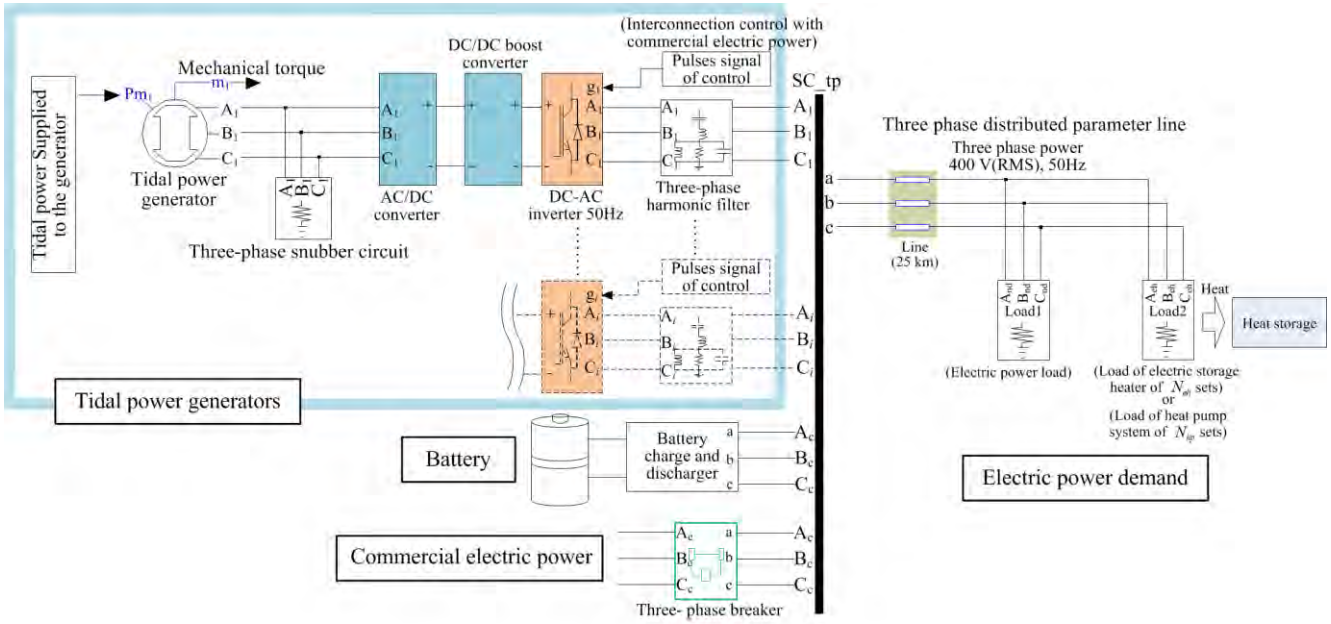

Fig. 4

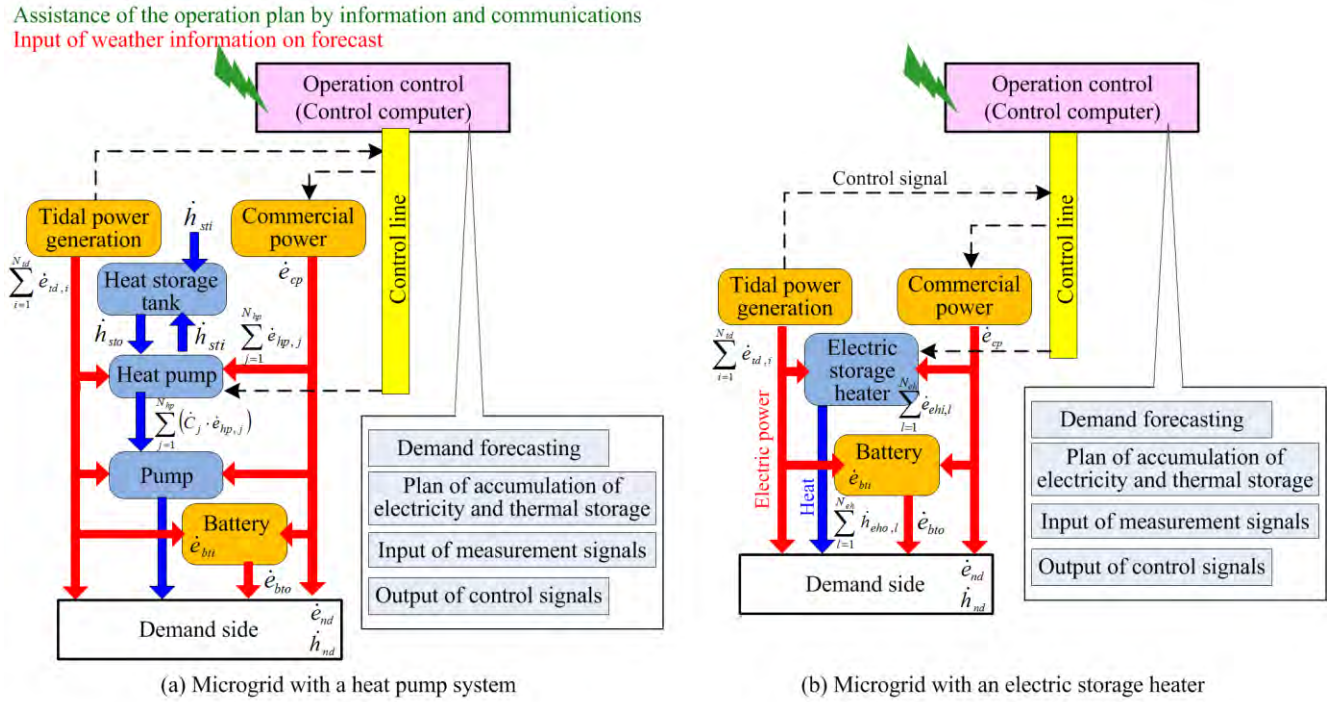

(a) Microgrid with a heat pump system

(b) Microgrid with an electric storage heater

Fig. 5

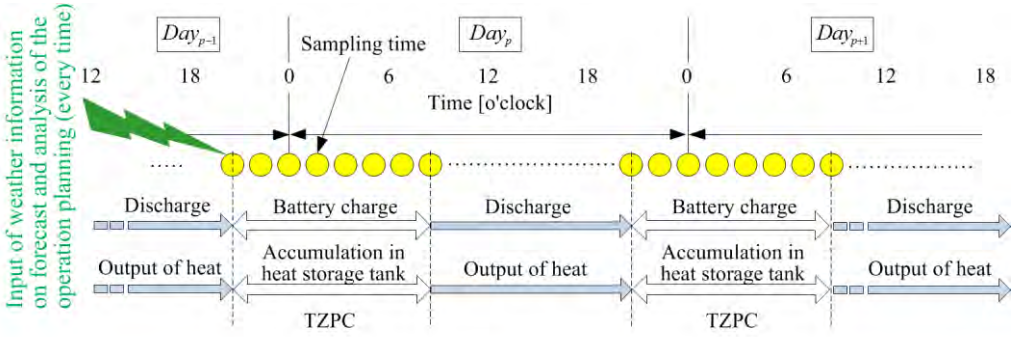
Input of weather information on forecast and analysis of the operation planning (every time)
Day p-1
Sampling time
Day p
Day p+1
12
18
0
6
12
18
0
6
12
18
Time [o'clock]
Discharge
Battery charge
Discharge
Battery charge
Discharge
Output of heat
Accumulation in heat storage tank
Output of heat
Accumulation in heat storage tank
Output of heat
TZPC
TZPC

Fig. 6

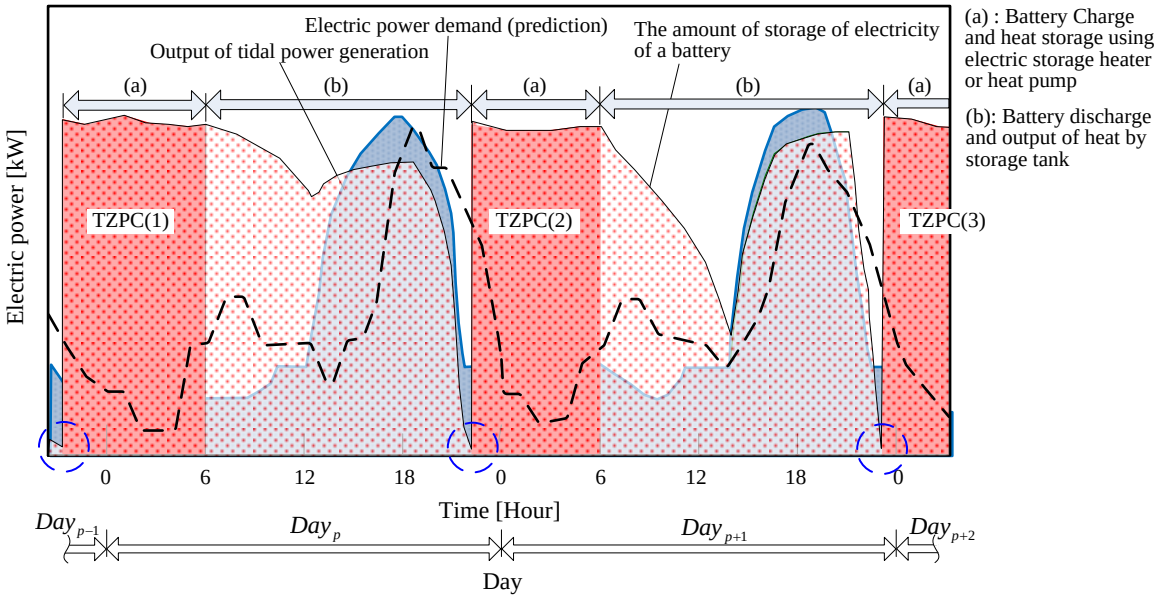
Electric power demand (prediction)
Output of tidal power generation
The amount of storage of electricity of a battery
(a)
(b)
(a)
(b)
(a)
(a) : Battery Charge and heat storage using electric storage heater or heat pump
(b): Battery discharge and output of heat by storage tank
Electric power [kW]
TZPC(1)
TZPC(2)
TZPC(3)
0
6
12
18
0
6
12
18
0
Time [Hour]
Day p-1
Day p
Day p+1
Day p+2
Day

Fig. 7

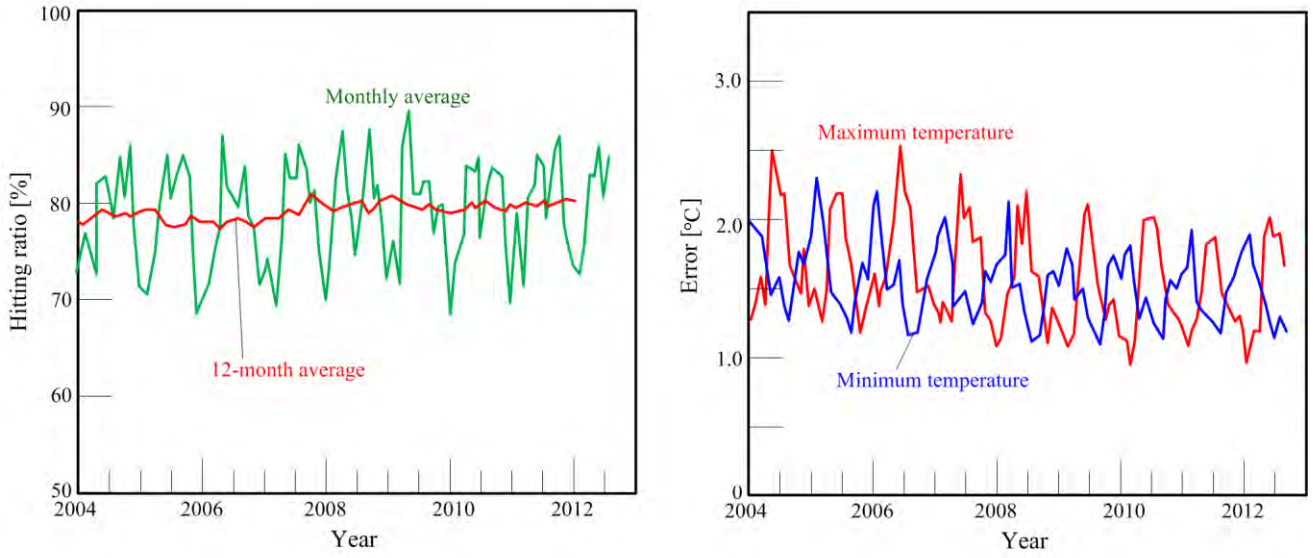
Hitting ratio [%]
100
90
80
70
60
50
Monthly average
12-month average
2004
2006
2008
2010
2012
Year
Error [°C]
3.0
2.0
1.0
0
Maximum temperature
Minimum temperature
2004
2006
2008
2010
2012
Year

Fig. 8

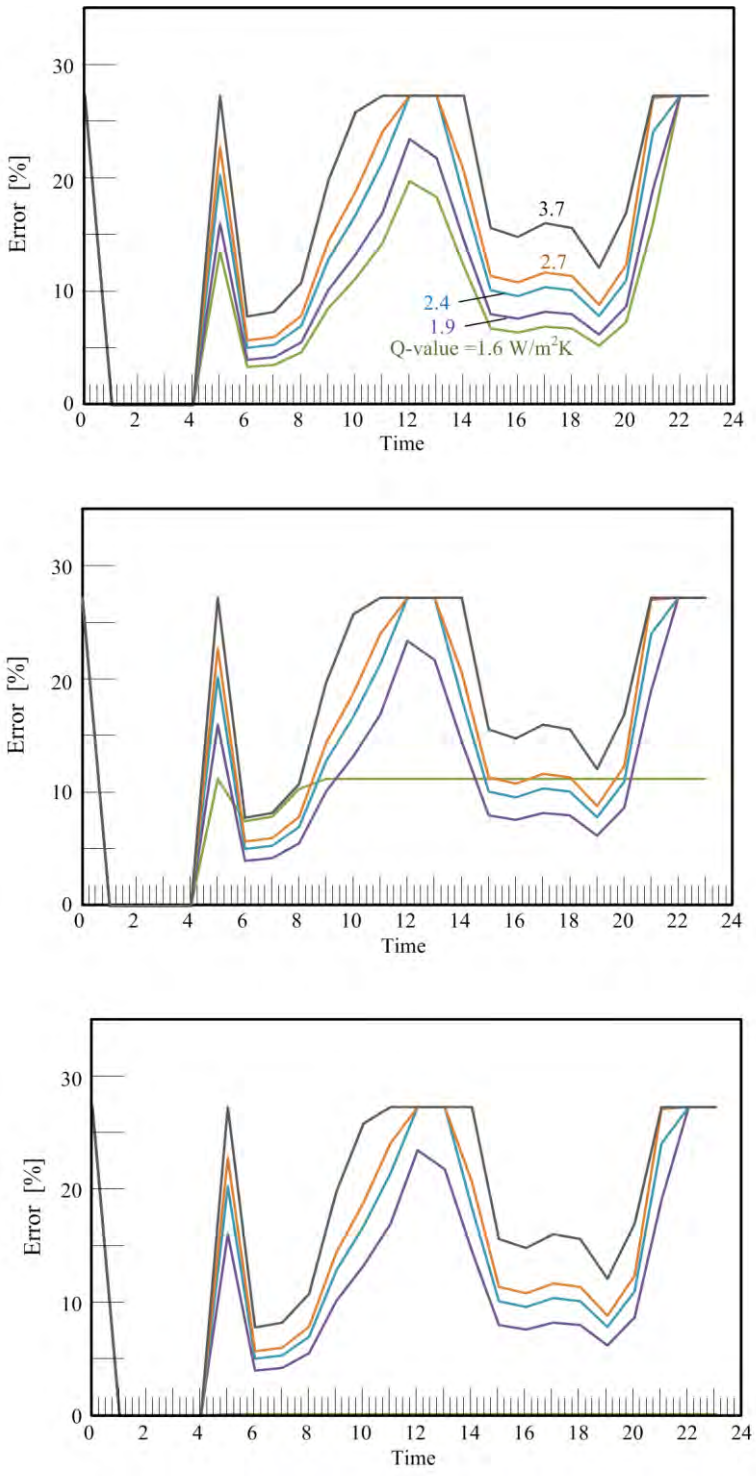

Fig. 9

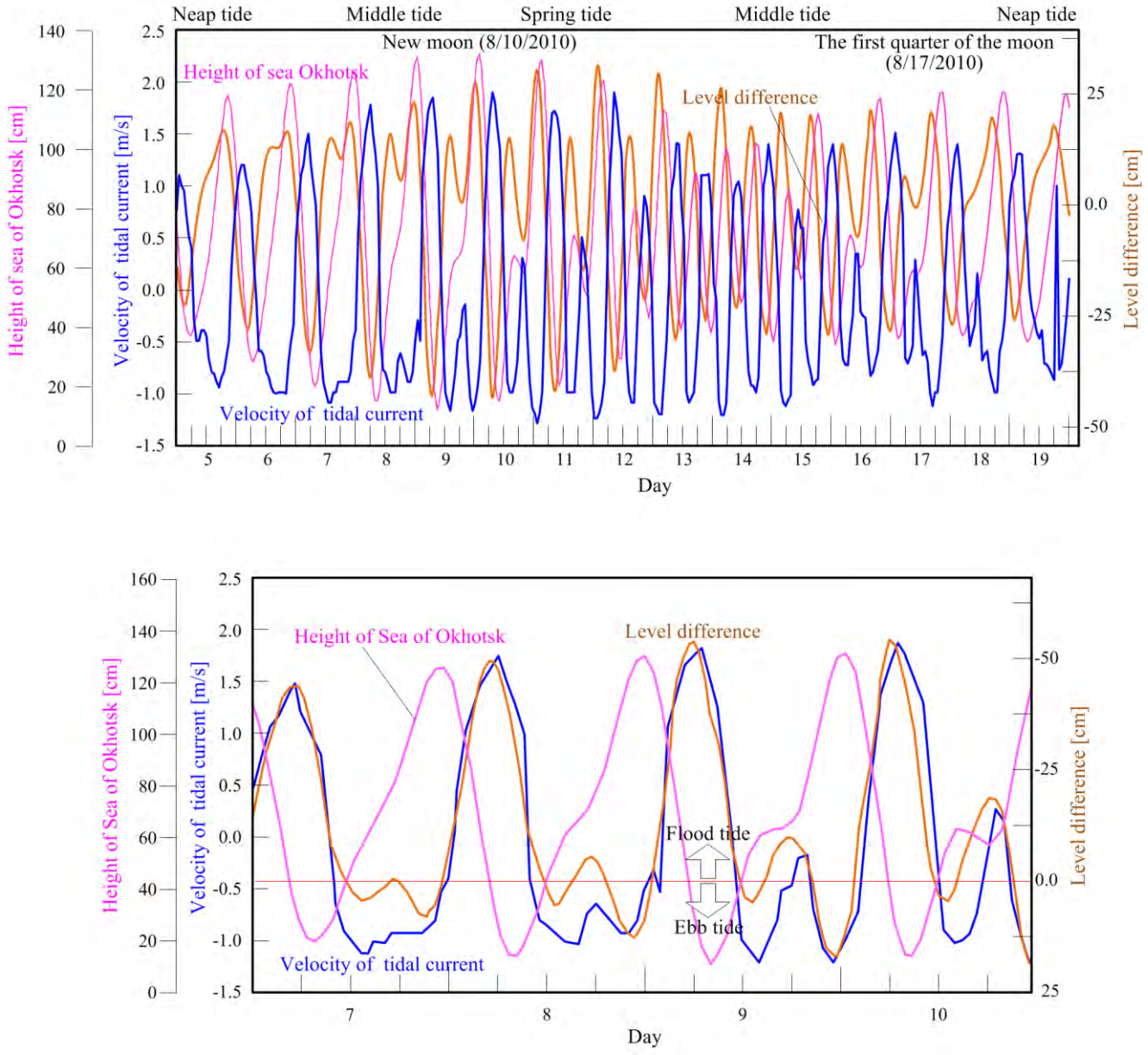
Neap tide
Middle tide
Spring tide
Middle tide
Neap tide
New moon (8/10/2010)
The first quarter of the moon
(8/17/2010)
Height of sea Okhotsk
Level difference
Velocity of tidal current
Height of sea of Okhotsk [cm]
Velocity of tidal current [m/s]
Level difference [cm]
Day
Height of Sea of Okhotsk
Flood tide
Ebb tide

721 Fig. 10

722

723

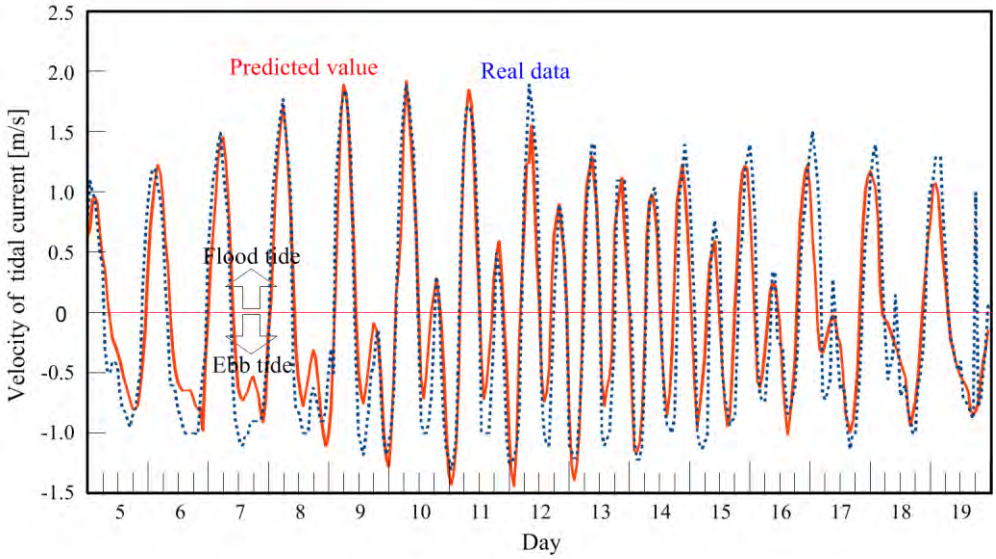

724

725

726

727

728

729

730

731

732

733

734

735

736

737

738

739

740

741

742

743 Fig. 11

744

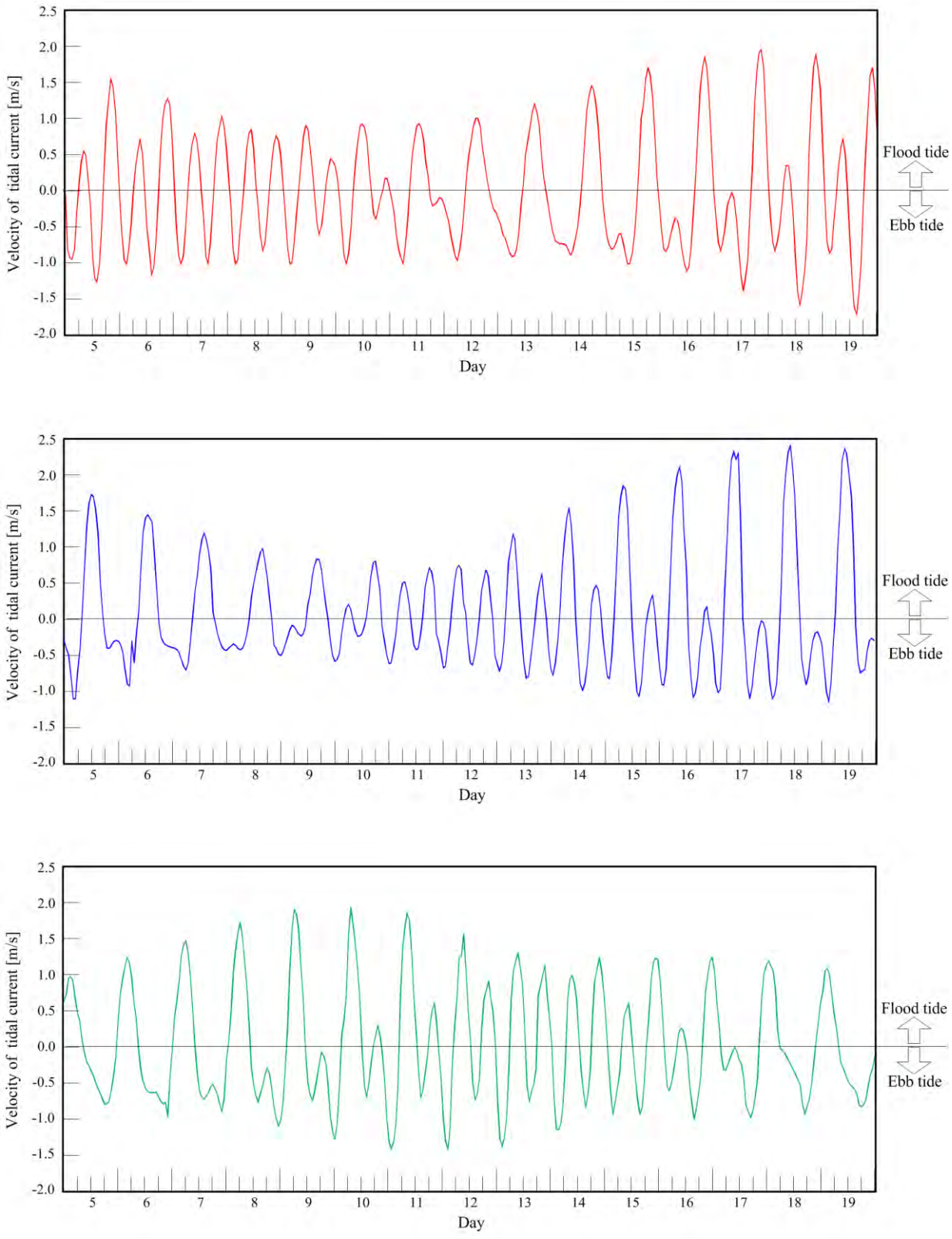

745

746

747 Fig. 12

748

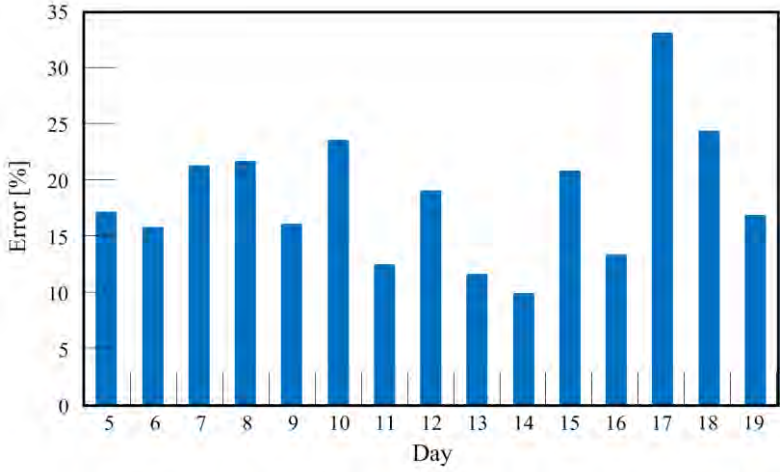

749

750

751 Fig. 13

752

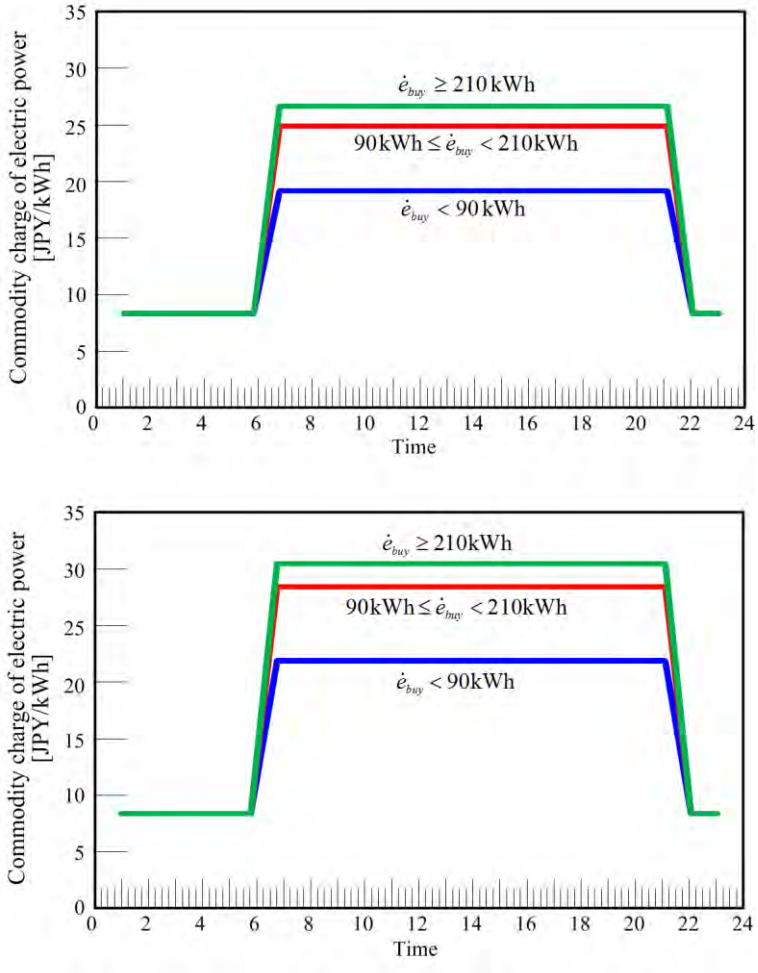

753

Fig. 14

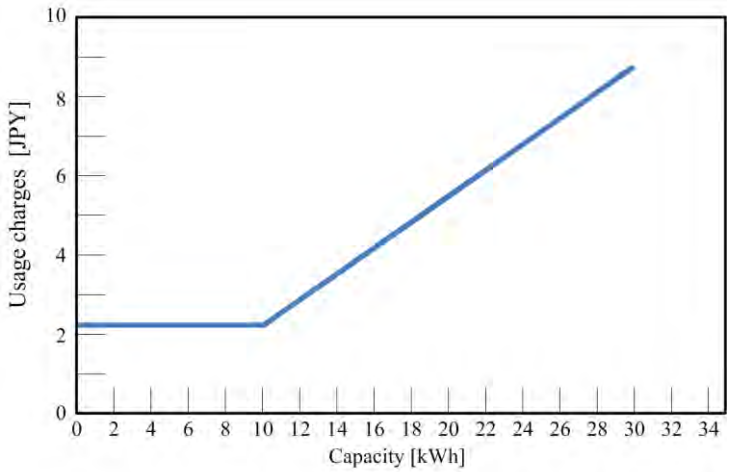
Usage charges [JPY]
Capacity [kWh]
0
2
4
6
8
10
0 2 4 6 8 10 12 14 16 18 20 22 24 26 28 30 32 34

Fig. 15

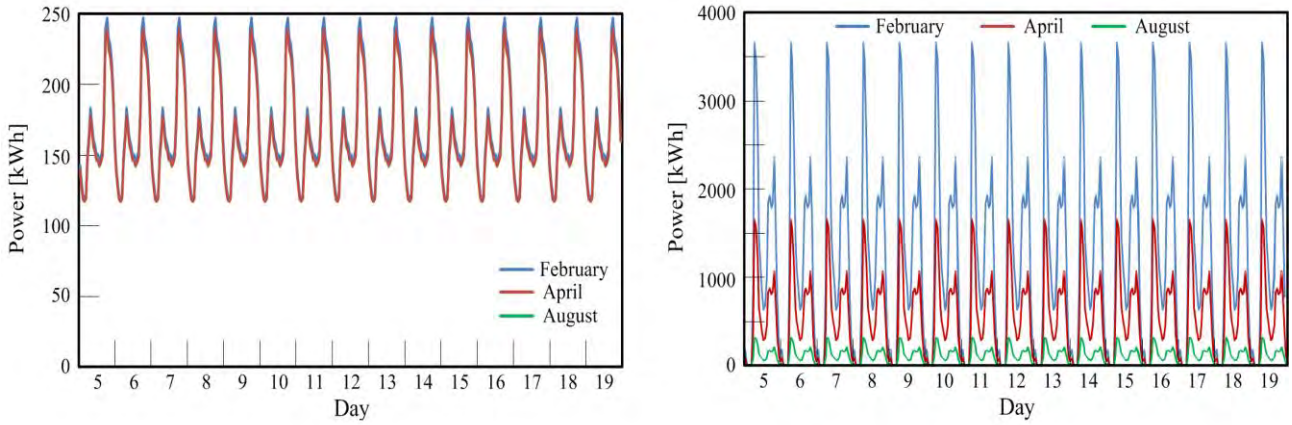
Power [kWh]
Day
February
April
August
0
50
100
150
200
250
5 6 7 8 9 10 11 12 13 14 15 16 17 18 19
Power [kWh]
Day
February
April
August
0
1000
2000
3000
4000
5 6 7 8 9 10 11 12 13 14 15 16 17 18 19

770 Fig. 16

771

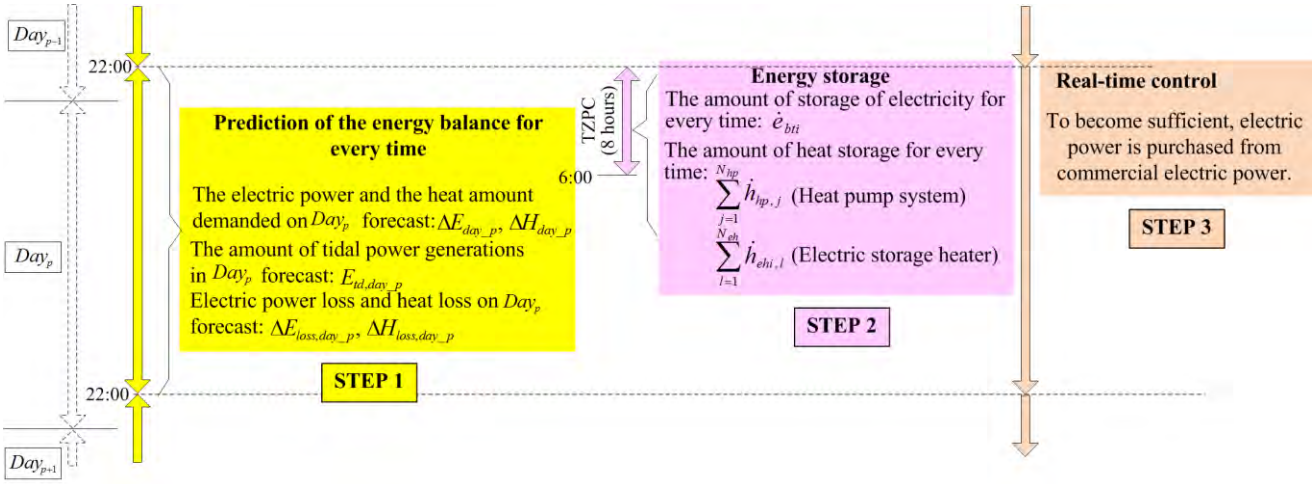

772

773

774

775 Fig. 17

776

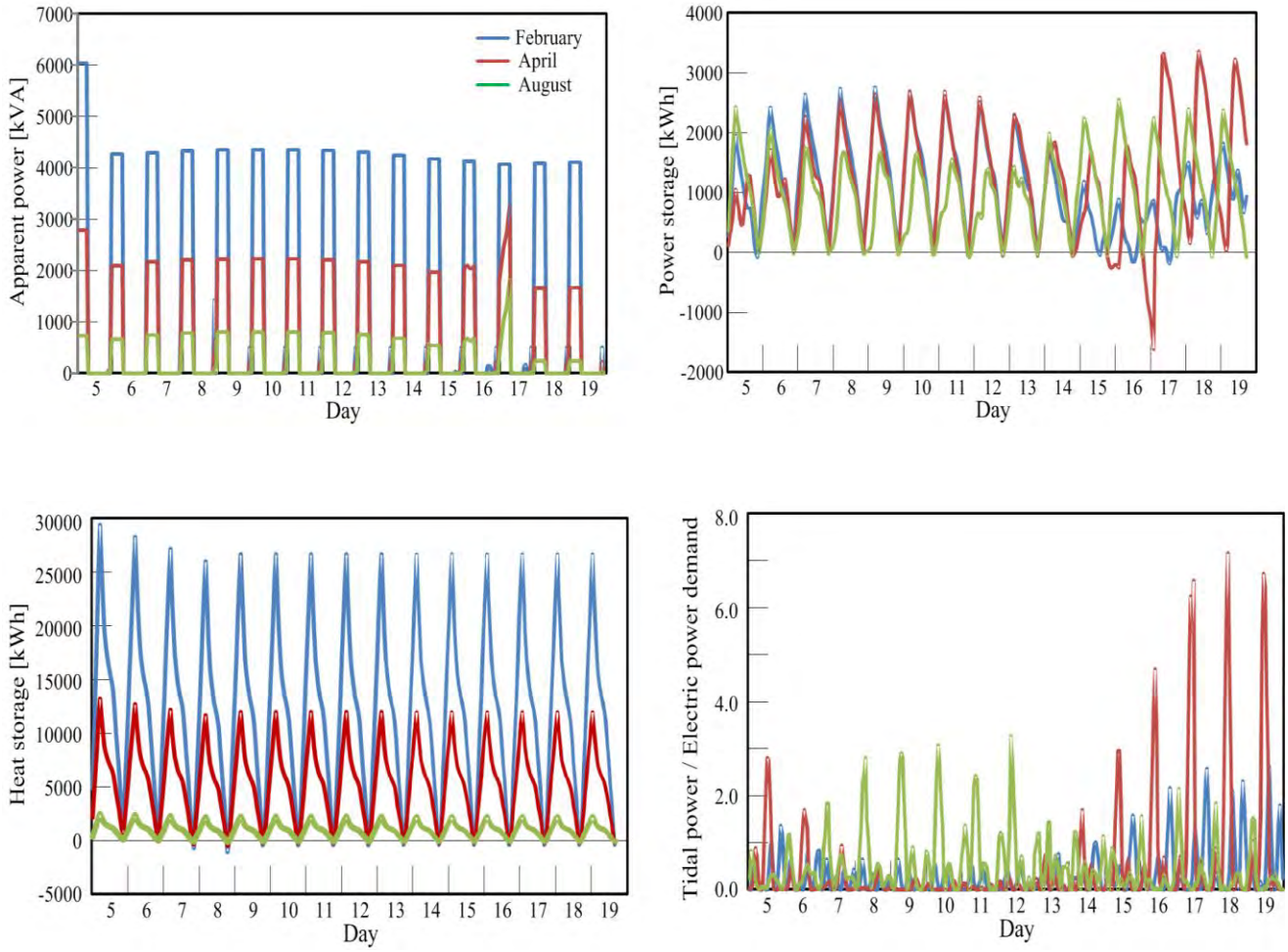

777

778

779

Fig. 18

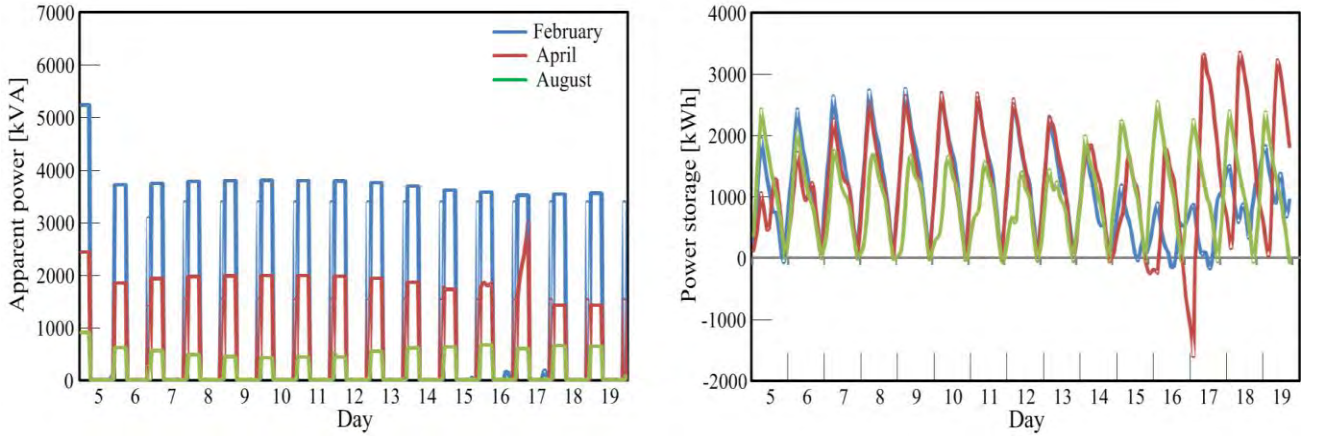
February
April
August
Apparent power [kVA]
Power storage [kWh]
Day
Day

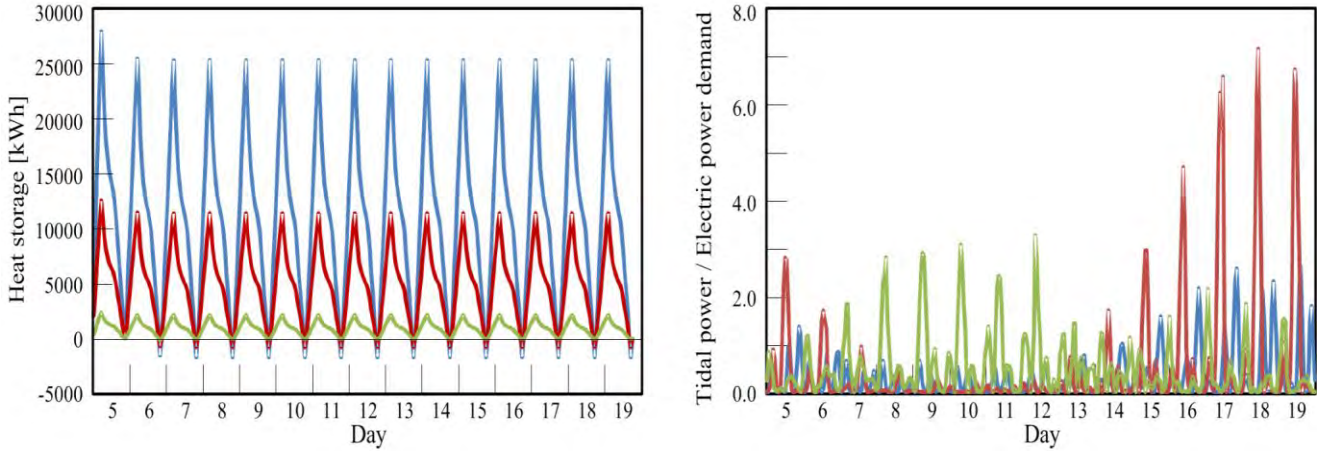
Heat storage [kWh]
Tidal power / Electric power demand
Day
Day

Fig. 19

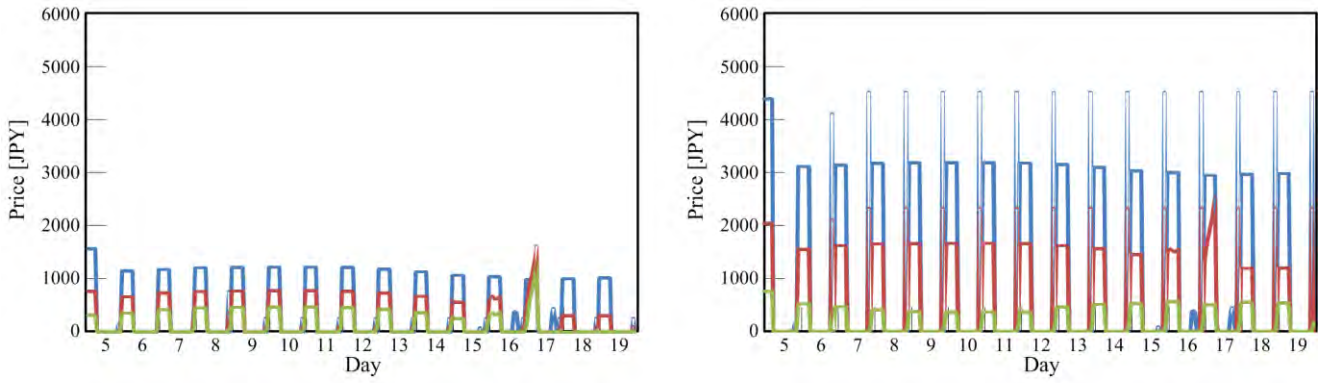
Price [JPY]
Price [JPY]
Day
Day

Fig. 20

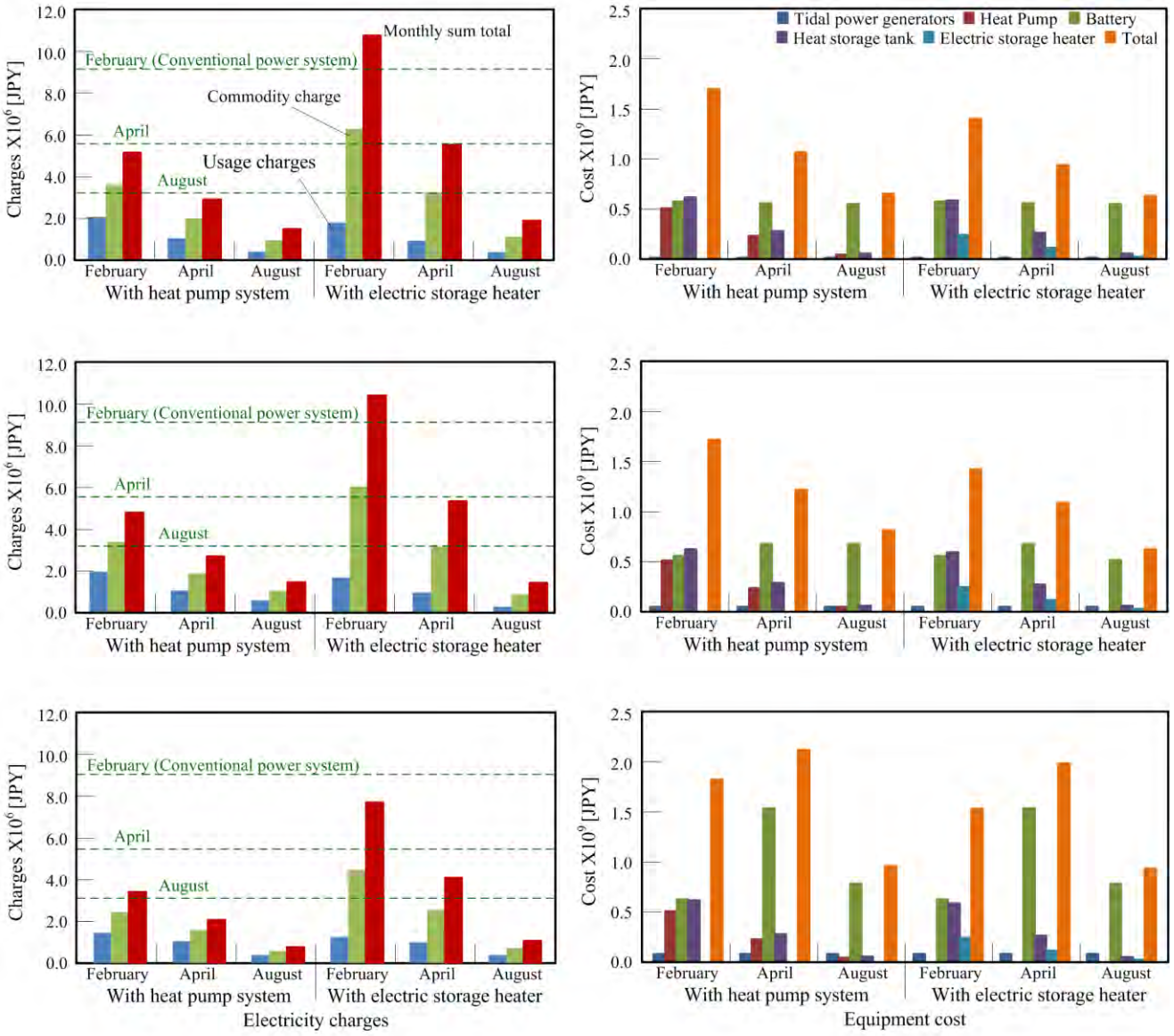
Charges X10^6 [JPY]
Monthly sum total
February (Conventional power system)
Commodity charge
April
Usage charges
August
February
April
August
With heat pump system
With electric storage heater
Cost X10^9 [JPY]
Tidal power generators
Heat Pump
Battery
Heat storage tank
Electric storage heater
Total
Charges X10^9 [JPY]
Cost X10^9 [JPY]
Charges X10^6 [JPY]
Cost X10^9 [JPY]
Electricity charges
Equipment cost

Fig. 21

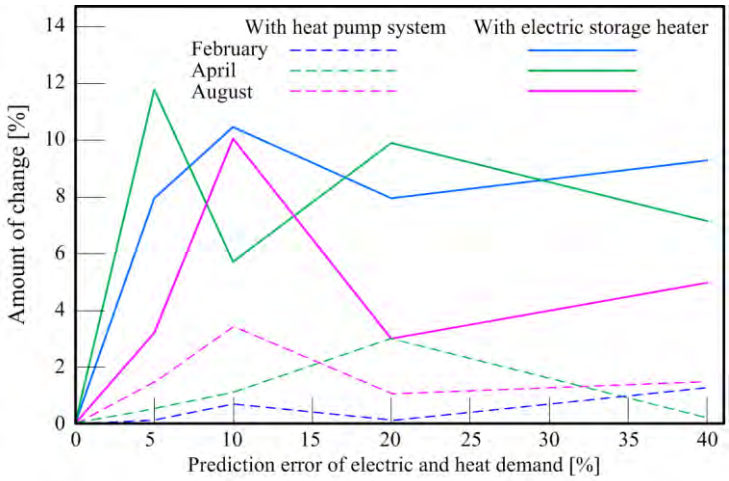
With heat pump system
With electric storage heater
February
April
August
Amount of change [%]
Prediction error of electric and heat demand [%]
0
2
4
6
8
10
12
14
0
5
10
15
20
25
30
35
40

Fig. 22

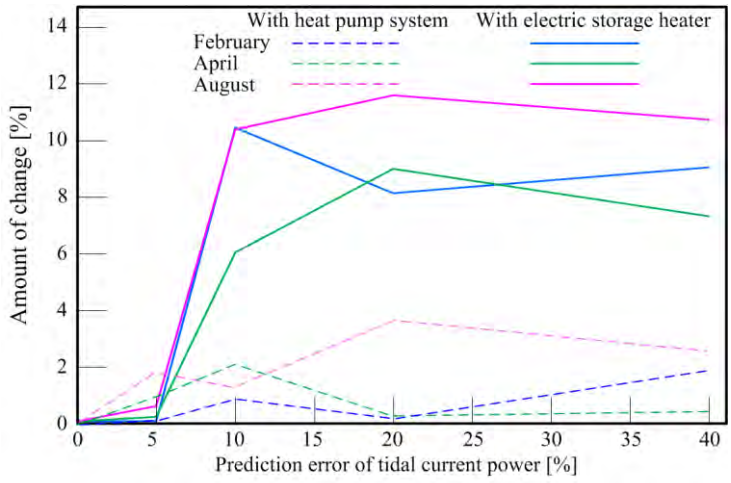
With heat pump system
With electric storage heater
February
April
August
Amount of change [%]
Prediction error of tidal current power [%]
0
2
4
6
8
10
12
14
0
5
10
15
20
25
30
35
40

Table 1

Turbine efficiency:	0.35
Diameter of hydraulic turbine:	2.4 m
Number of hydraulic turbine:	20-200 sets
Loss of heat storage tank:	5%/Day
Coefficient of charge and discharge of battery:	0.85
Self-discharge of battery:	0.5%/Day
Power conditioner:	0.9
COP of heat pump:	3.5
Power factor of heat pump:	0.9
Power transmission loss of power grid:	0.0
Loss of heat supply to heat grid:	0.0

Table 2

Tidal power generator	400,000 JPY/kW
Heat pump	100,000 JPY/kW
Battery	200,000 JPY/kWh
Heat storage tank	21,000 JPY/kWh
Electric storage heater	50,000 JPY/kWh

JPY = Japanese yen